Supplementary Material

Mechanistic understanding of 3d-metal phthalocyanine catalysts: heterostructure regulation of the dz^2 states for efficient CO_2 reduction

The zero-point energy and entropy

The zero-point energy contribution is obtained from the vibrational contribution to internal thermal energy (Equations 1-2), and further simplified to Equation 3. Vibrational frequencies

$$E_{ZPE} = K_B \sum_K \theta_{f,\kappa} \left(\frac{1}{2} - \frac{1}{e^{\theta_{f,\kappa}/T} - 1} \right) \quad (1)$$

$$\theta_{f,\kappa} = \frac{\hbar f_\kappa}{K_B} \quad (2)$$

$$E_{ZPE} = \frac{1}{2} K_B \sum_K \theta_{f,\kappa} \quad (3)$$

$$S = K_B \sum_K \left(\frac{\theta_{f,\kappa}/T}{e^{\theta_{f,\kappa}/T} - 1} - ln(1 - e^{-\theta_{f,\kappa}/T}) \right) \quad (4)$$

(f_K) are taken from VASP, with those below 24.80 m eV (200 cm^{-1}) normalized to that value in order to avoid errors associated with the harmonic oscillator model. The entropy contribution is computed as the vibrational entropy (S) (Equation 4) for all gases except CO_2, O_2 and H_2, for which the standard entropy value is taken from literature as the experimental entropy in the gas phase at standard conditions[1].

Work function:

Work function values were obtained using symmetric models without dipole correction to avoid the artefactual effects of the asymmetric slab model on the average local potential within the vacuum. The work function was calculated as the difference between the Fermi level and the average local potential of electrons in the vacuum ($\Phi = \varepsilon_V - \varepsilon_F$).

Molecular Dynamics:

Most of the existing electrocatalytic CO_2RR is carried out at room temperature[2]. In order to simulate the real experimental reaction conditions, we choose the canonical ensemble (NVT) with constant temperature for molecular dynamics simulation[3]. The *ab initio* molecular

dynamic (AIMD) simulations were carried out to evaluate the thermodynamic stability using the NVT ensemble at 300 K for 5ps with a 1 *fs* time step.

Arrhenius equation:

In 1889, on the basis of a large number of experimental results, Aaronius proposed the following empirical formula:

$$\frac{dlnk}{d_T} = \frac{E_a}{RT^2} \tag{5}$$

$$E_a = RT^2 \frac{dlnk}{d_T} = -R \frac{dlnk}{d_{\frac{1}{T}}} \tag{6}$$

An indefinite integral of the differential form of Arrhenius can be obtained:

$$lnk = \frac{-E_a}{RT} + C \tag{7}$$

The Arrhenius formula can also introduce a pre-exponential factor (also known as frequency factor) A. Let C = lnA :

$$lnk = \frac{-E_a}{RT} + lnA \tag{8}$$

Take the exponents of both sides and rewrite them as:

$$k = Ae^{-\frac{E_a}{RT}} \tag{9}$$

This formula indicates that the reaction rate constant is exponentially related to temperature.

It can be seen from Equation (7) that the plot of *lnk* to *1/T* should be a straight line. If the temperature is T_1 and T_2 respectively, the reaction rate constants are k_1 and k_2 respectively, then

$$lnk_1 = \frac{-E_a}{RT_1} + C \tag{10}$$

$$lnk_2 = \frac{-E_a}{RT_2} + C \tag{11}$$

From Equation (10) minus Equation (11):

$$ln\frac{k_2}{k_1} = \frac{-E_a}{R}\left(\frac{1}{T_2} - \frac{1}{T_1}\right) = \frac{-E_a T_1 - T_2}{R \quad T_1 T_2} \tag{12}$$

Geometric structure model

In this study, we evaluated the electrocatalytic properties of 3d-TMPc for CO_2RR and studied various structural changes to improve their performance. Based on the Kohn-Sham equation and previous studies suggested that any interaction between atoms can be disregarded if their distance exceeds 6Å[4].

We simplified the computational simulation structure of the phthalocyanine (Pc) molecule, as depicted in Fig. S1(a).

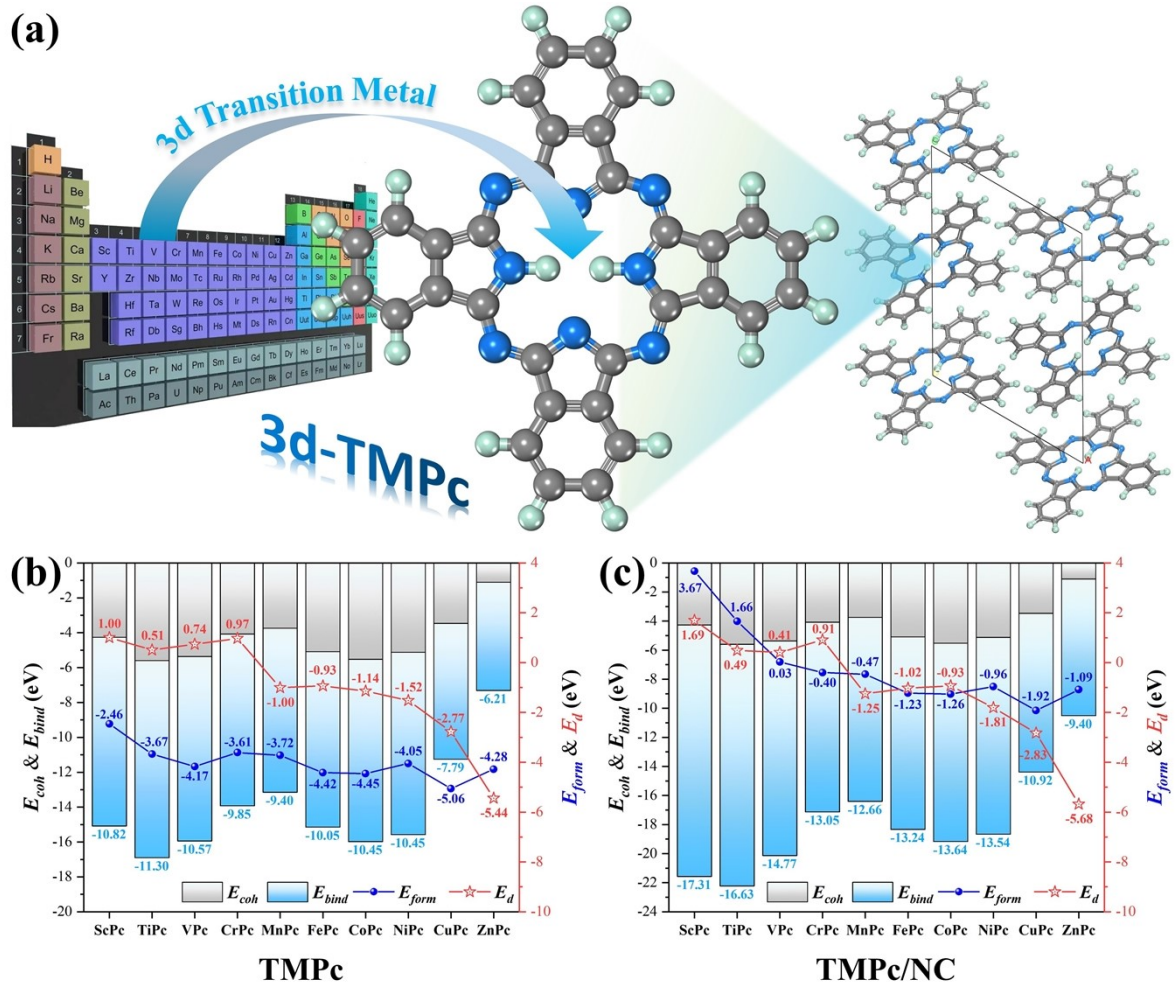

Fig. S1 (a) The schematic diagram of structural model construction of 3d-TMPc catalyst. (b-c) The cohesive energy (E_{coh}) and binding energy (E_{bind}) of each 3d-TMPc or 3d-TMPC/NC structure. The red and blue dot-line diagrams are the *d*-band center and formation energy of each 3d-TMPC or 3d-TMPC/NC, respectively.

To investigate the stability of the central metal in 3d-TMPc catalyst, we initially calculated the binding energy (E_{bind}) of 3d-TMPc and the cohesive energy (E_{coh}) of the metal species. The E_{bind} refers to the energy required to bond the Pc molecule with the transition metal, while E_{coh} refers to the energy required to keep the metal bulk together. These values were obtained using Formulas (13) and (14), respectively, as shown in Fig. 1(b).

$$E_{bind} = E_{total} - E_{single} - E_{Pc} \tag{13}$$

$$E_{coh} = \frac{E_{bulk}}{n} - E_{single} \tag{14}$$

Where, E_{total}, E_{single}, E_{Pc},and E_{bulk} represent the total energy of 3d-TMPc, the energy of a single transition metal atom, the energy of a phthalocyanine molecule, and the energy of the excessive metal bulk, respectively. While n refers to the number of metal atoms in bulk.

Figure 1(b) displays the binding energy of the central metal atoms in our chosen model catalysts to the Pc structure. The E_{bind}, which is more negative than the E_{coh} of the corresponding metal bulk, indicates that the central metal atoms are firmly coordinated with the Pc structure, making it difficult for them to agglomerate. The results demonstrate that all central metals in Pc structures have a more negative E_{bind} than the E_{coh} of the corresponding central metal bulk, suggesting that they are stably coordinated with the Pc structure rather than being agglomerated. From Fig. S1(c), we find that the E_{bind} in 3d-TMP_C/NC heterostructures is more negative than that in 3d-TMPc (Specific data are shown in Table S1). Therefore, the central metals of 3d-TMPc homogeneous and 3d-TMPc/NC heterostructures catalysts have excellent stability, which is consistent with previous reports. Fig. S3 and Fig. S4 depict the structure optimization models for all 3d-TMPc catalysts and their corresponding electron localization function (ELF). The optimized structure model reveals that the Sc atom protrudes from the 3d-TMPc monolayer to form a rectangular pyramid structure with four other N atoms, while the other nine 3d-TMPc molecules exhibit a single planar structure. In addition, we also investigated the d-band center of each metal site. According to the d-band center theory, we can preliminarily predict that MnPc, FePc and CoPc may have superior catalytic activity due to their comparatively favorable d-band centers. Furthermore, the d-band center of the 3d-TMPc/NC heterostructure change may increase the catalytic performance of the 3d-TMPc.

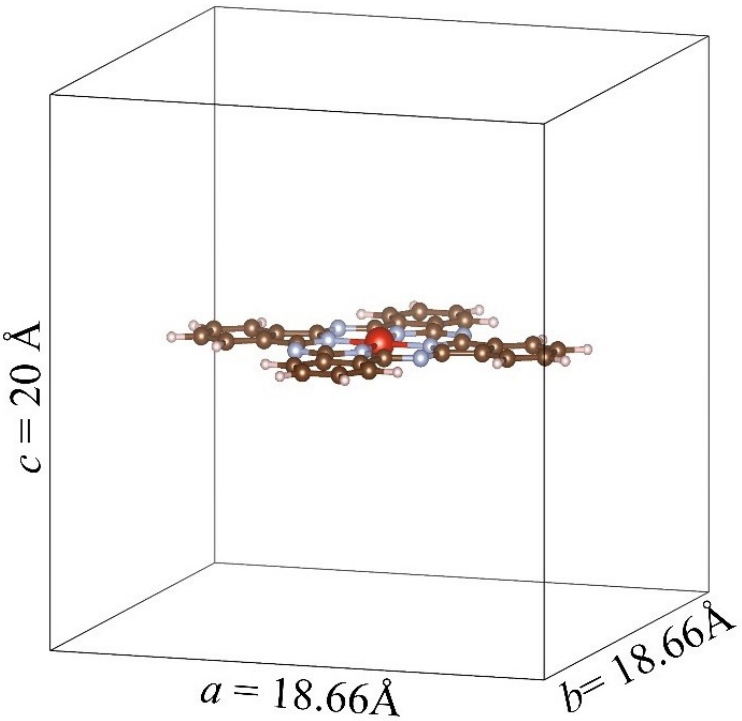

Fig. S2 The cell structure of the optimized phthalocyanine molecule doped with transition metals (TMPc). The pink, brown and light grey balls represent H, C and N, respectively, while the red ball are used for the transition metal.

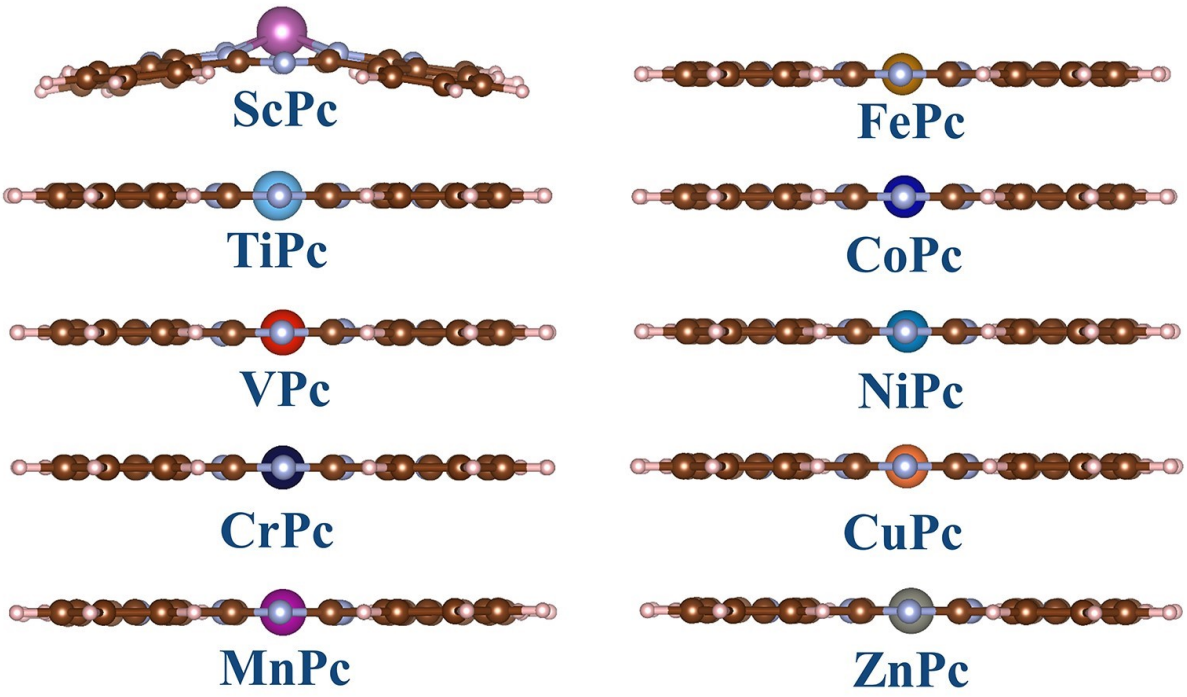

Fig. S3 The side view of the optimized structures of TMPc. The pink, brown and light grey balls represent H, C and N, respectively, while the other colors are used for the TM.

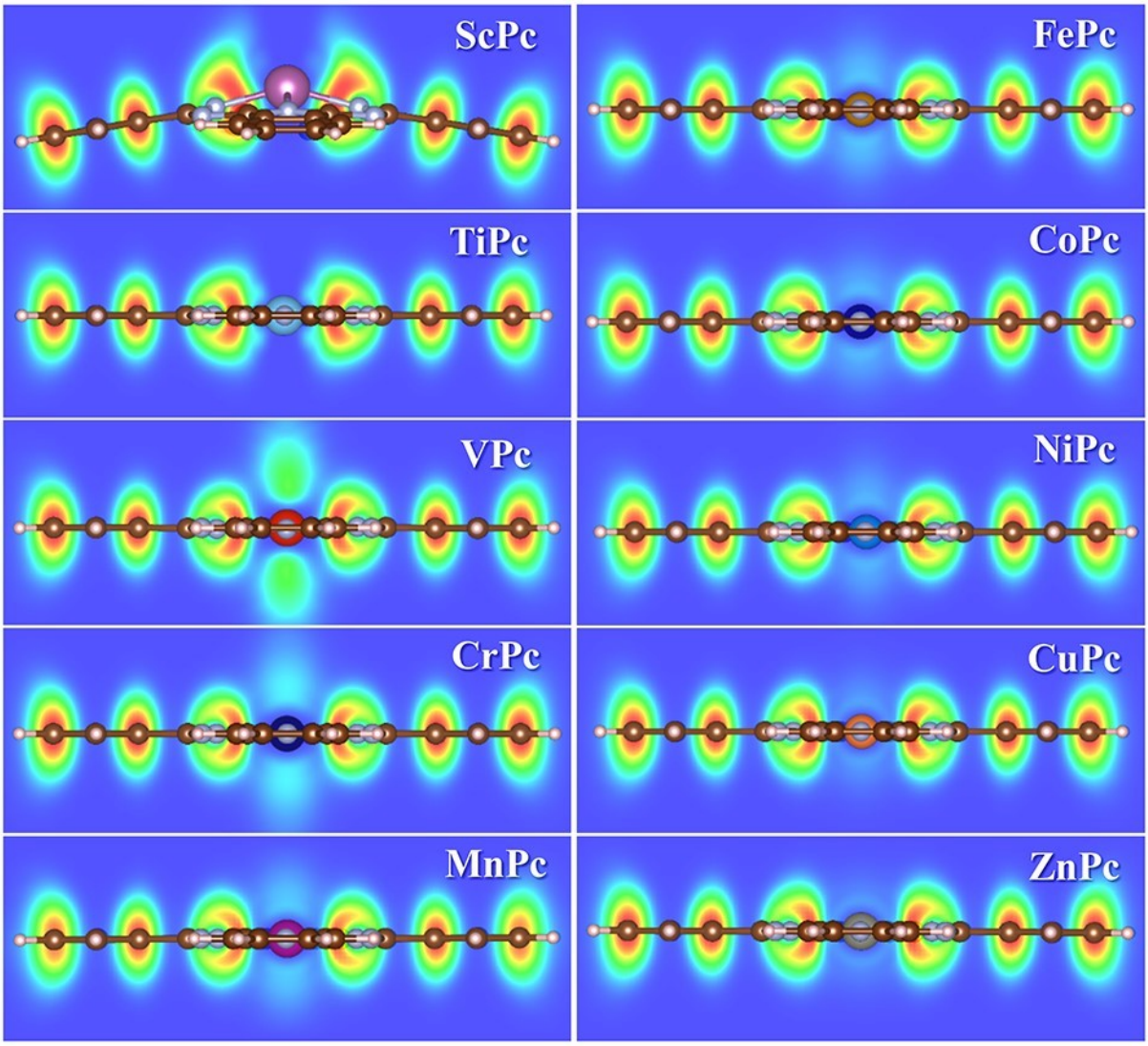

Fig. S4 (b) They are all 3d-TMPc models after geometry optimization, and their background charge clouds are electron localization functions (ELF) diagrams obtained by electron self-consistent calculation.

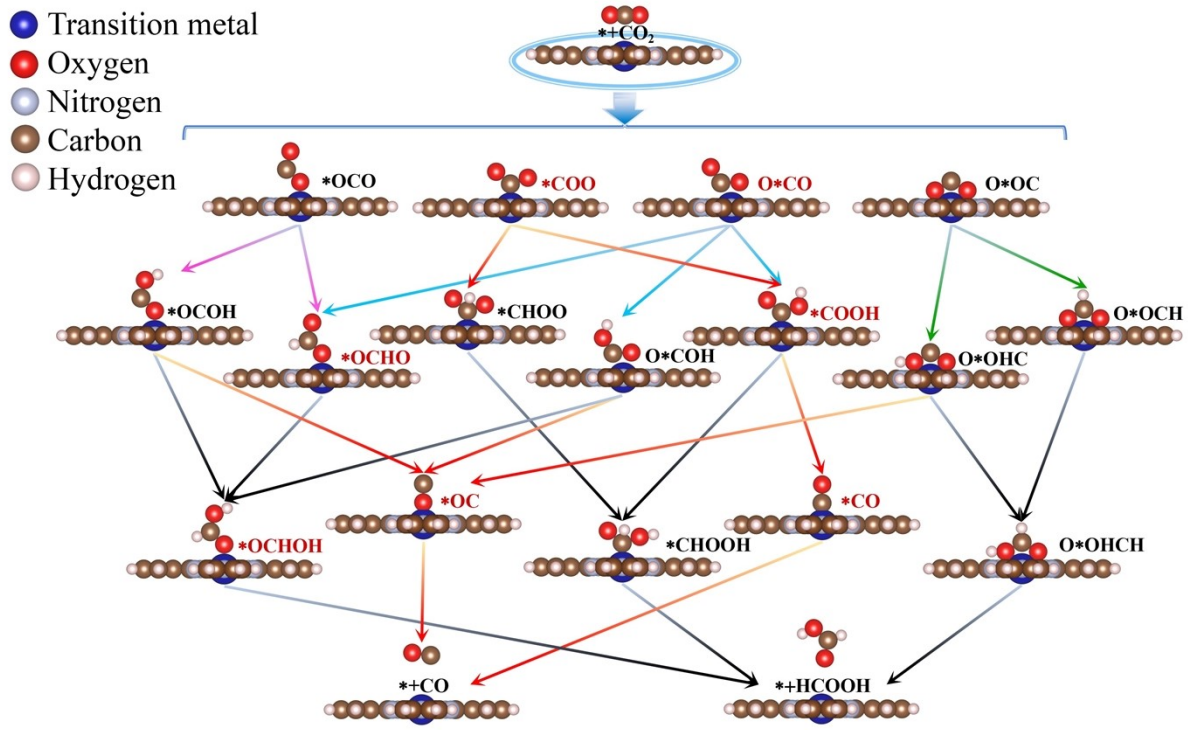

Fig. S5 The possible pathway and intermediates for electrocatalytic reduction of carbon dioxide to CO and HCOOH.

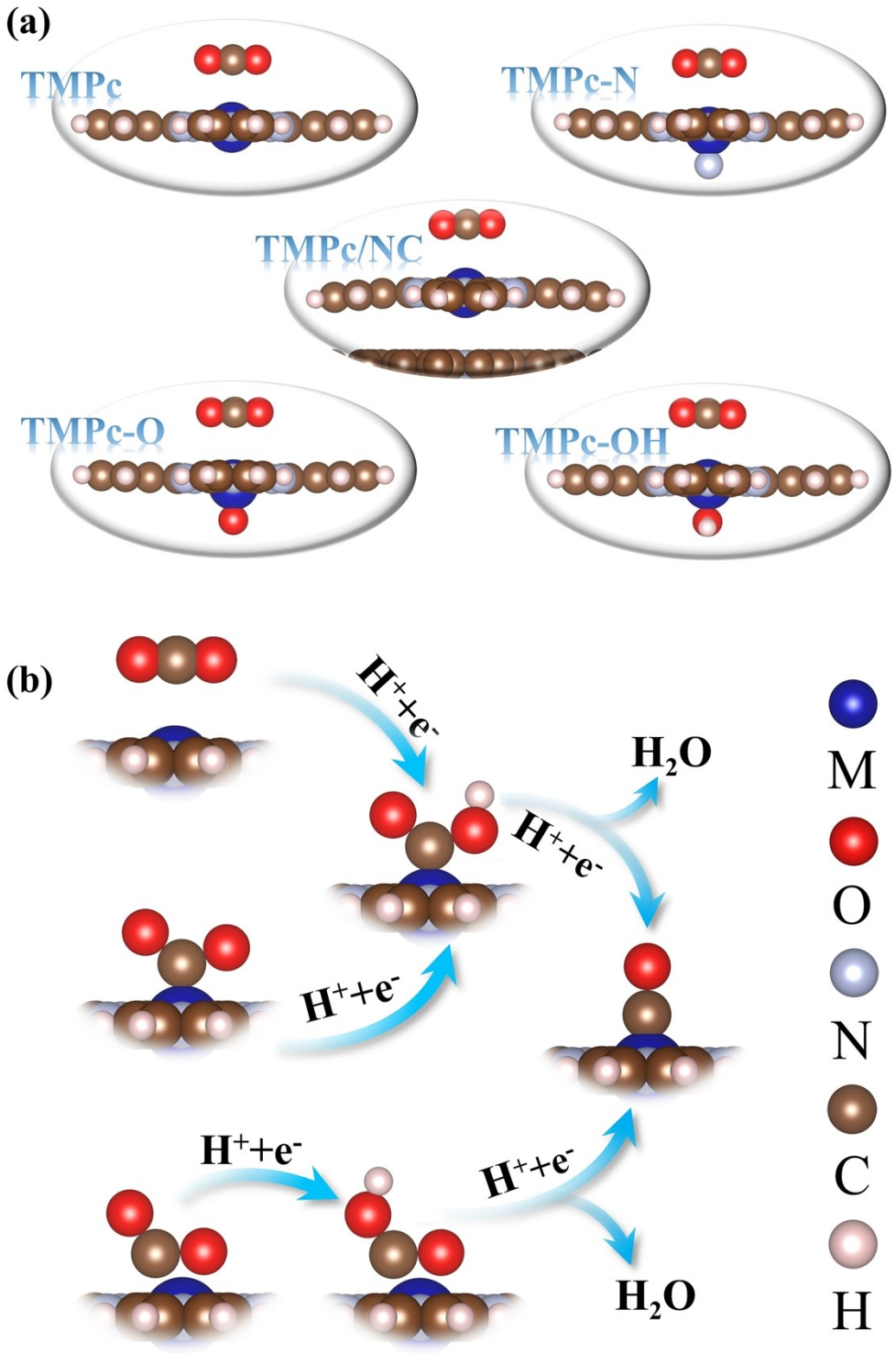

Fig. S6 (a) Five catalyst models: TMPc, TMPc with axial ligands including TMPc-O, TMPc-OH, TMPc-N, and a heterostructure TMPc/NC; (b) The main pathway of electrocatalytic CO_2RR conversion to CO on 3d-TMPc.

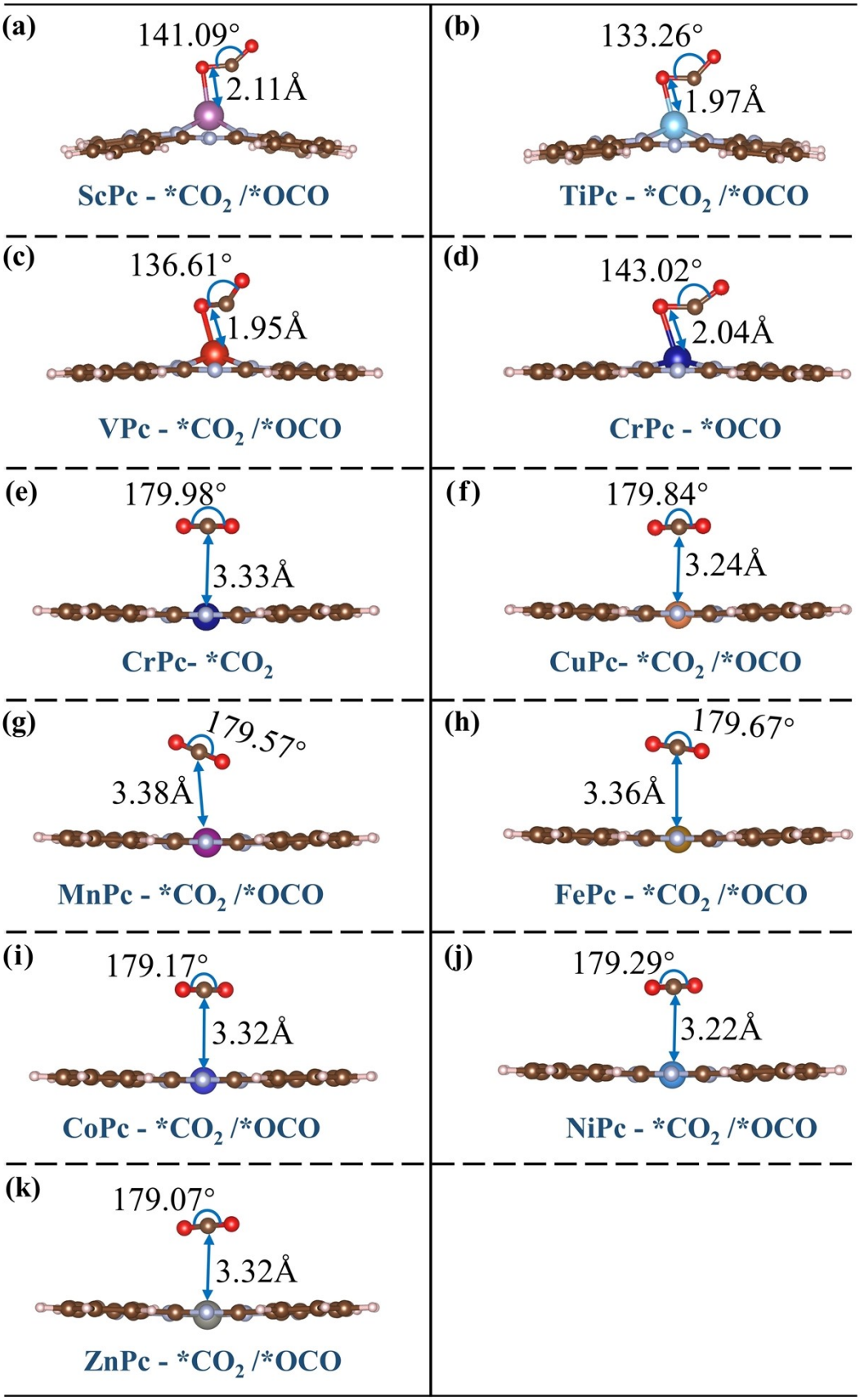

Fig. S7 The optimized structural models of ten 3d-TMPcs adsorbing CO_2 molecules.

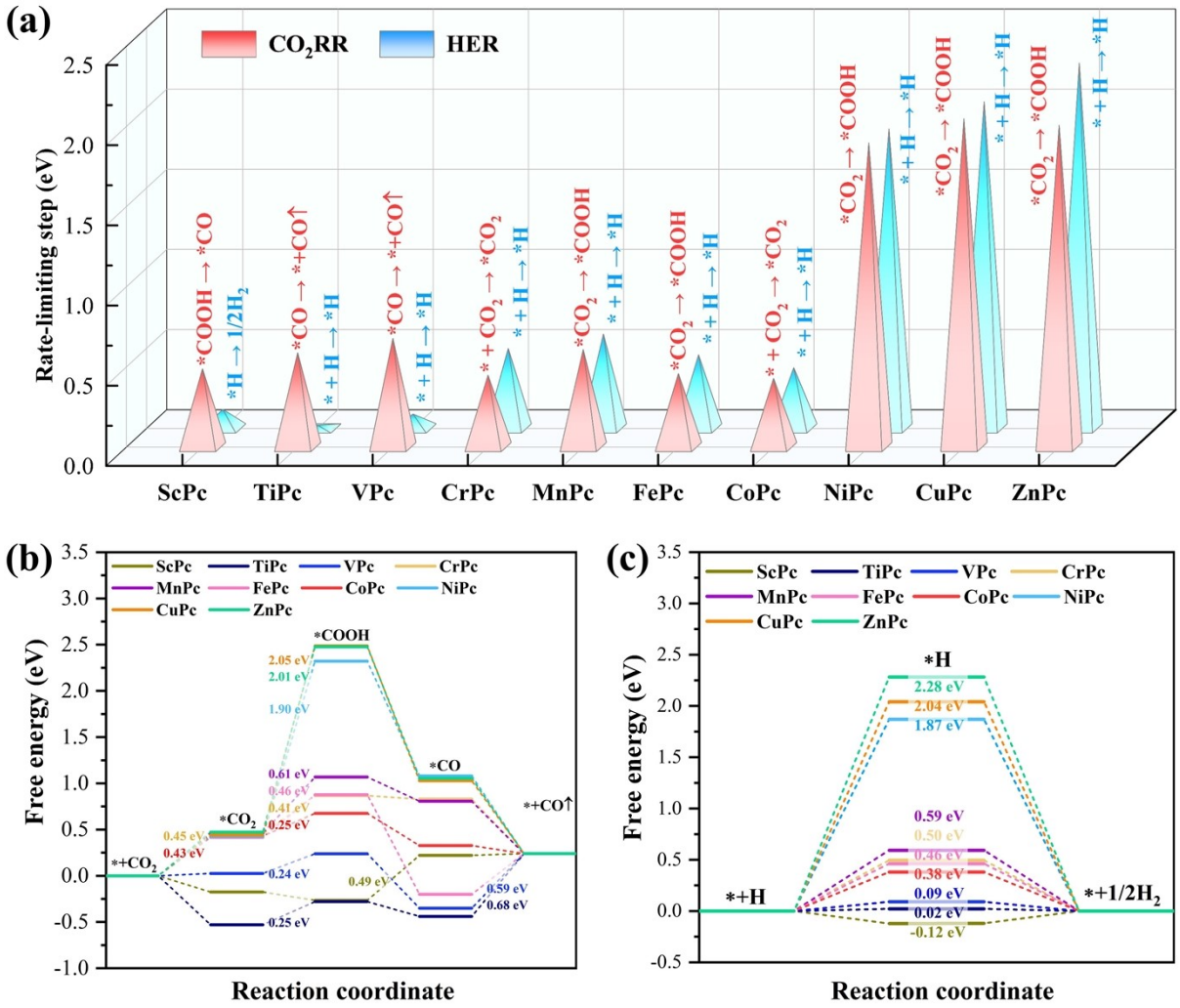

Fig. S8 (a) The RLS of the carbon dioxide reduction and hydrogen evolution reaction on various 3d-TMPc; (b) The free energy diagrams for CO products on 3d-TMPc; (c) The free energy diagrams for HER on 3d-TMPc.

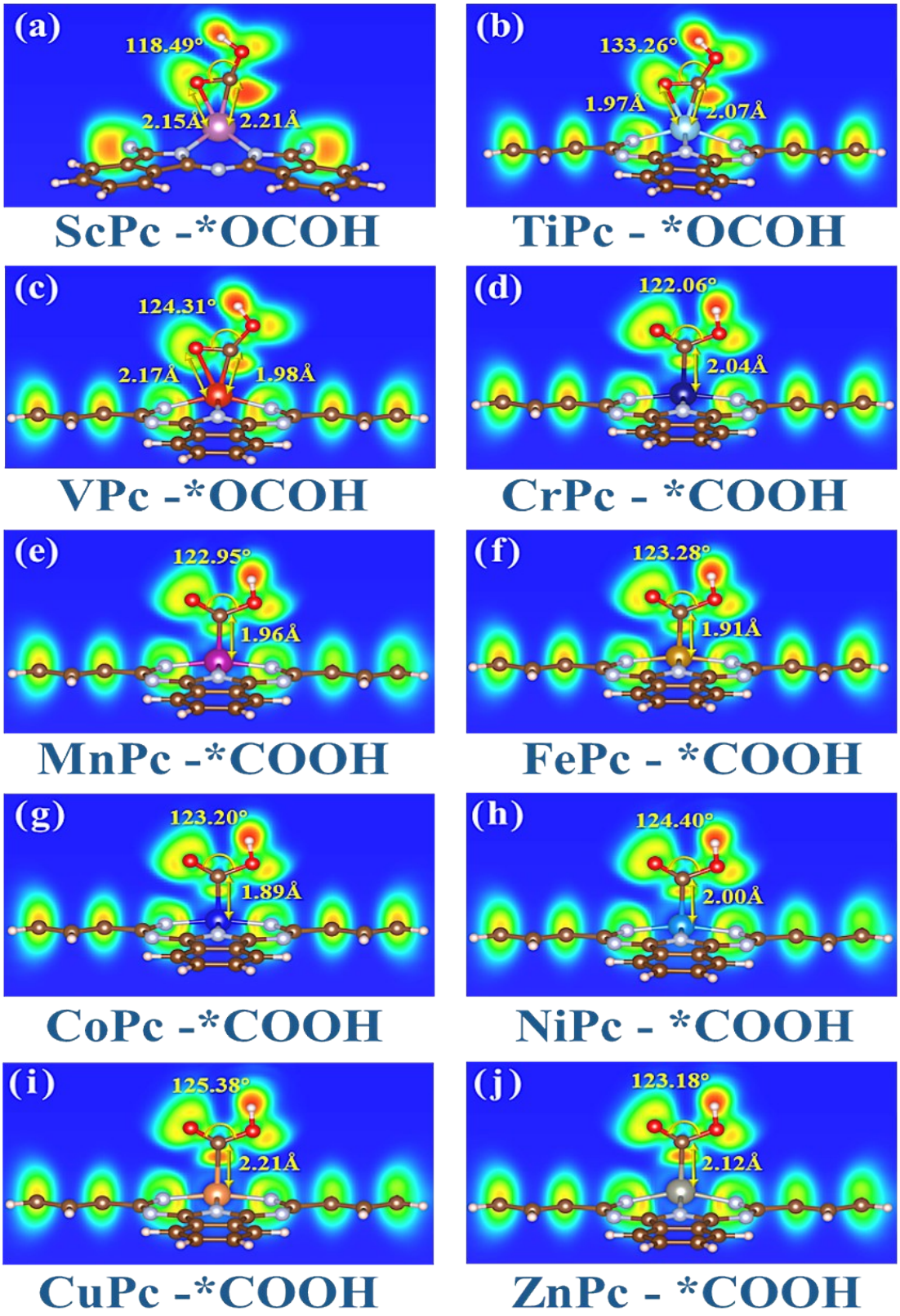

Fig. S9 The structural model for the formation of *COOH intermediates on all 3d-TMPc and the corresponding ELF. The bond length between C atom and metal center and the bond angle of O-C-O are also given.

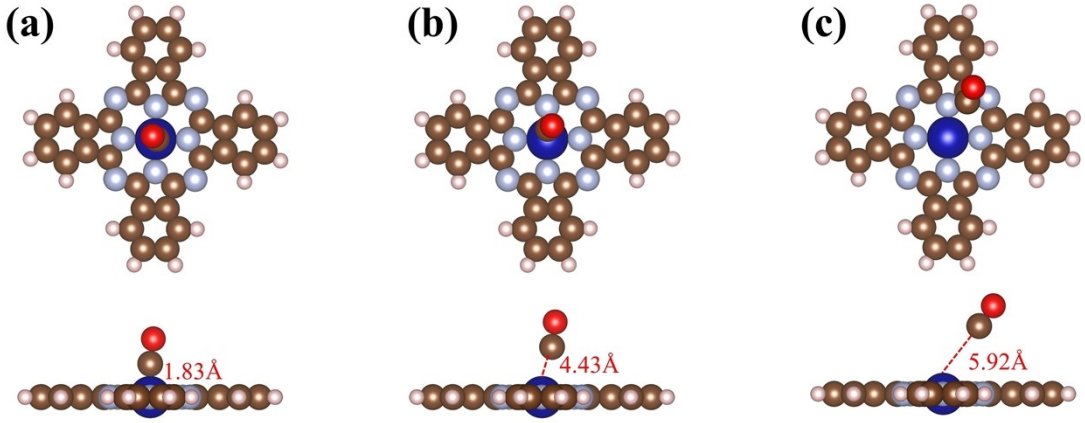

Fig. S10 The transition state model of CO desorption from the surface of 3d-TMPC catalyst, (a), (b) and (c) correspond to the initial state, transition state and final state, respectively.

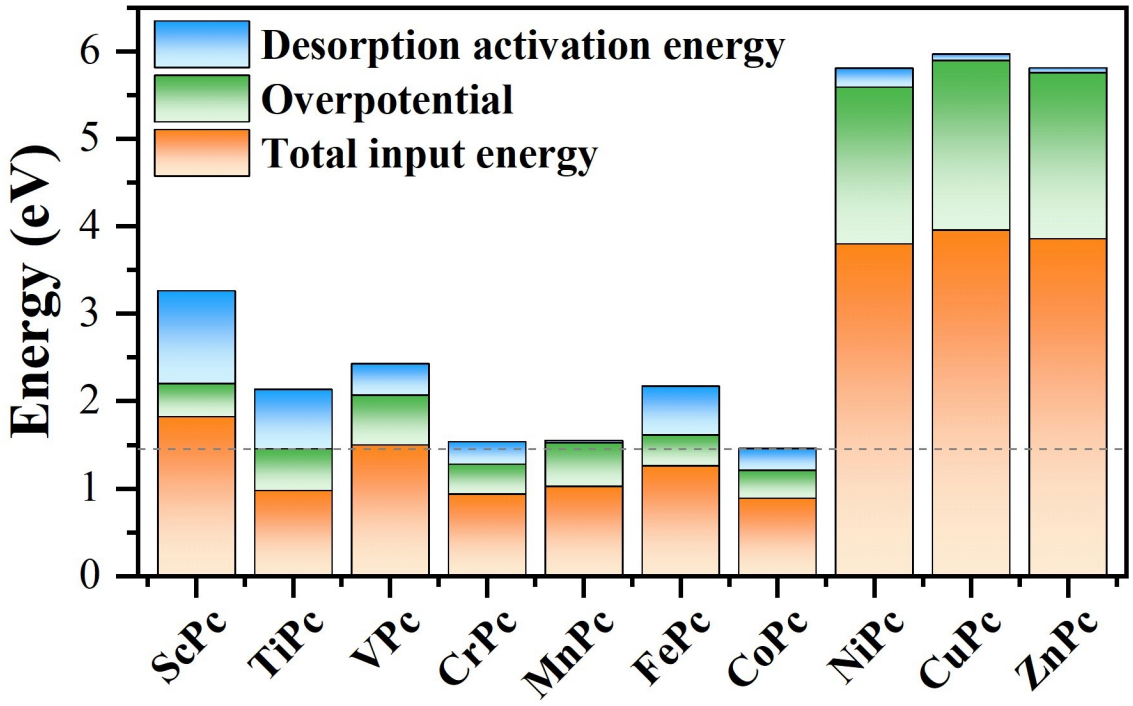

Fig. S11 The comparison of the overpotential energy, desorption activation energy and total input energy of CO_2RR electrocatalyzed with different 3d-TMPCs. (Since CO_2 to CO is a two-electron reaction step, we use the total energy required for the reaction E_{total} ($E_{total} = 2e\eta^{co} + E_a$) to measure the difficulty of generating the target product CO.)

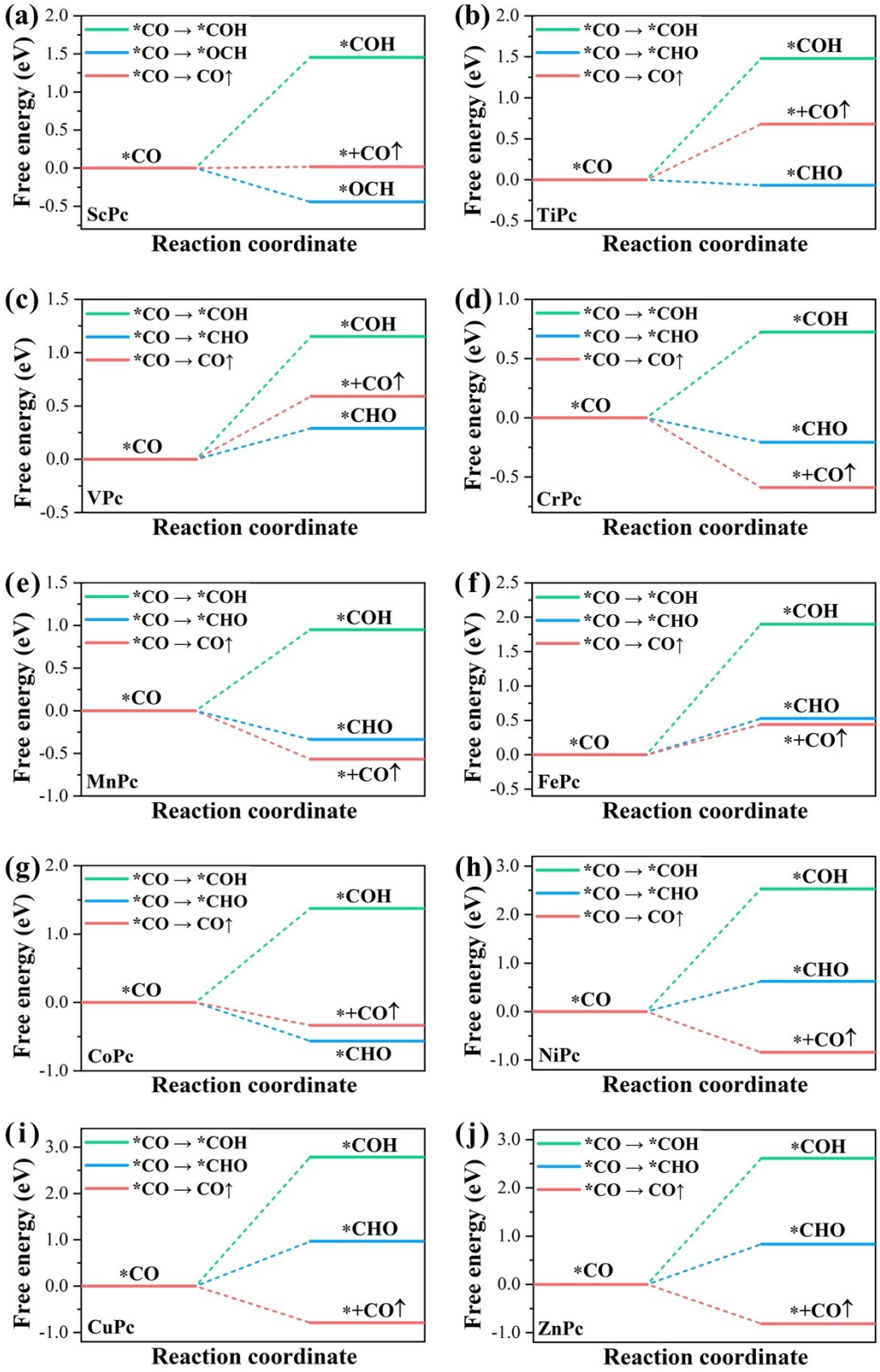

Fig. S12 The free energy of CO intermediate further hydrogenation to CHO and COH intermediates or product CO direct desorption on each 3d-TMPc catalyst.

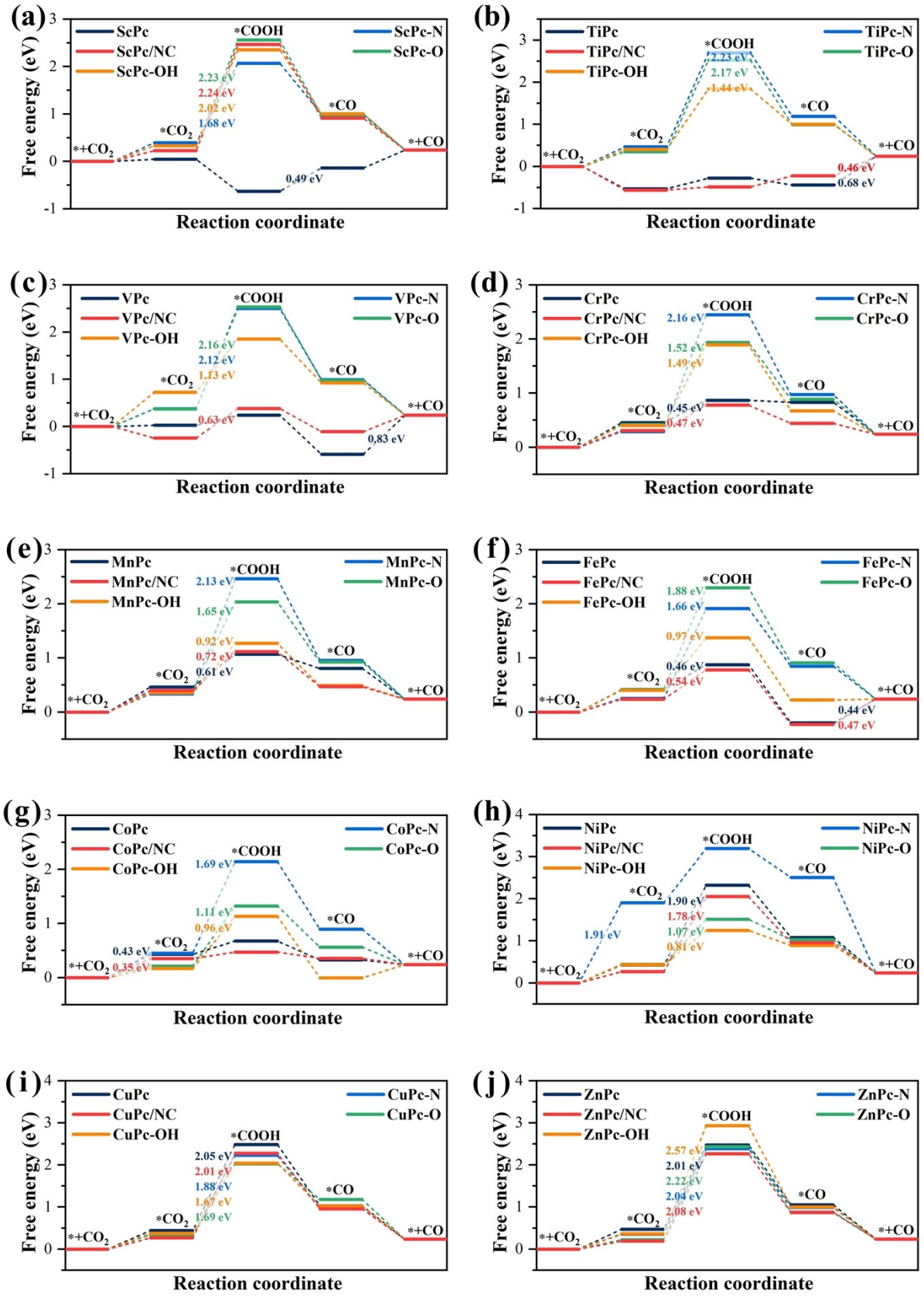

Fig. S13 Comparison of free energy under various axial ligands (O, OH and N) and pyridine nitrogen carbon substrate modification.

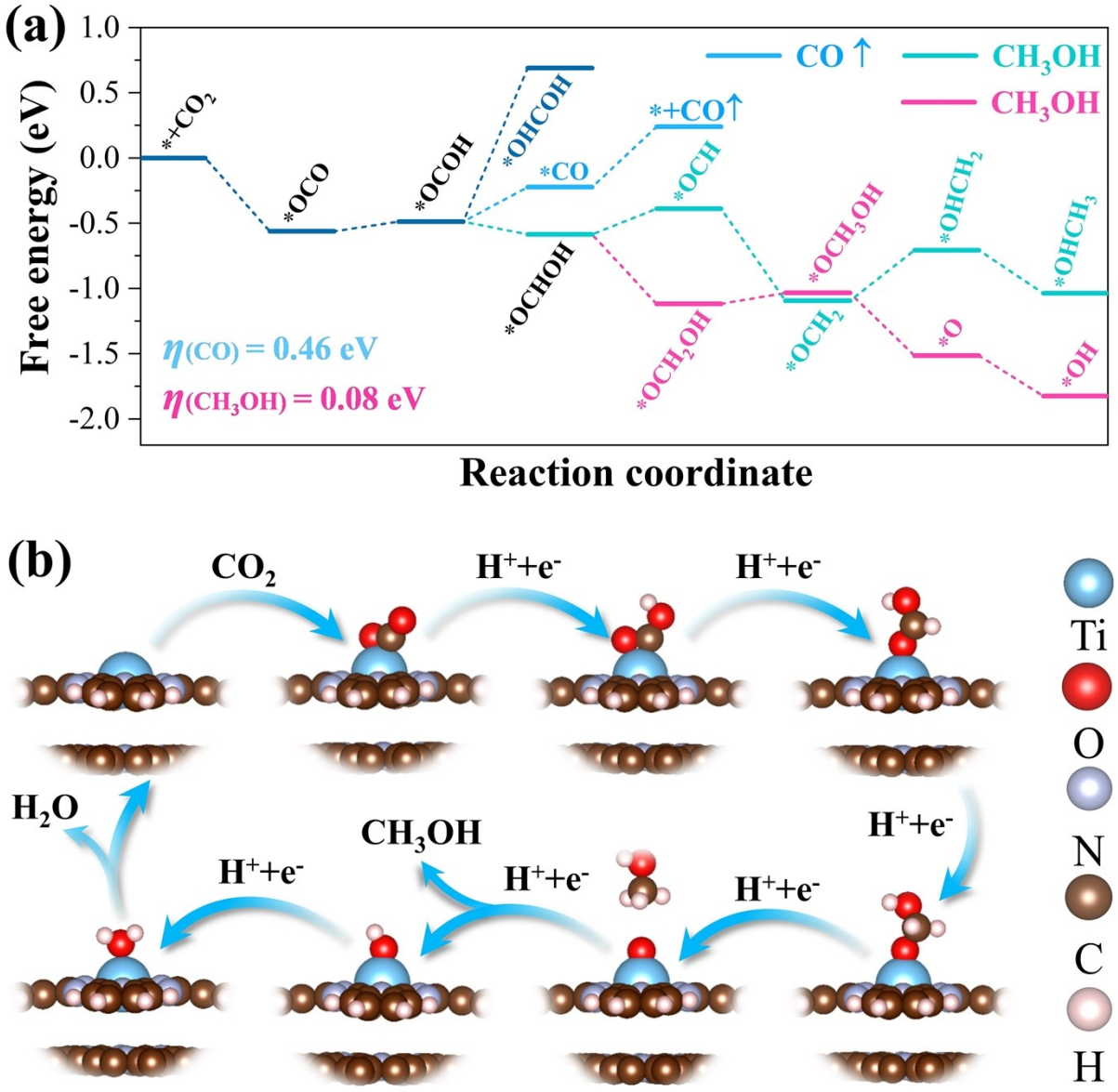

Fig. S14 (a) The free energy comparison diagram of electrocatalytic CO_2 to CO and CH_3OH conversion on TiPc/NC. (b) The reaction path and structure optimization model of electrocatalytic CO_2 conversion to CH_3OH on TiPc/NC.

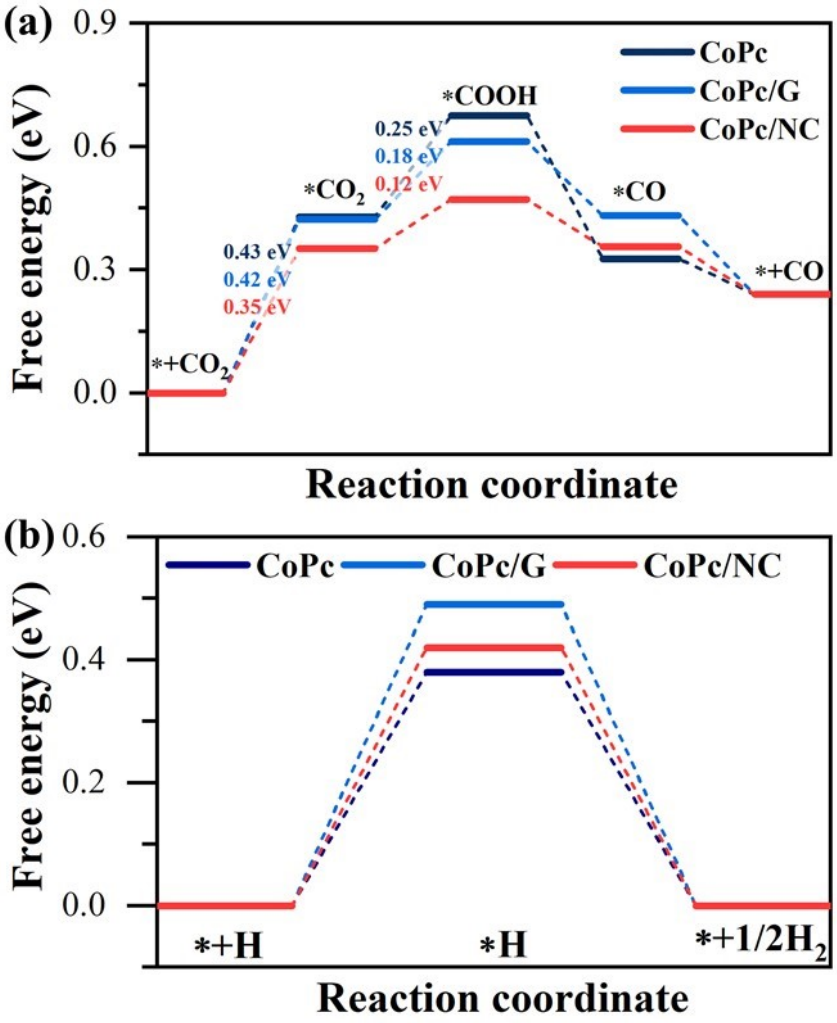

Fig.S15 (a) The free energy diagram of CoPc, CoPc/G and CoPc/NC. (b) The free energy diagrams for HER on CoPc, CoPc/G and CoPc/NC.

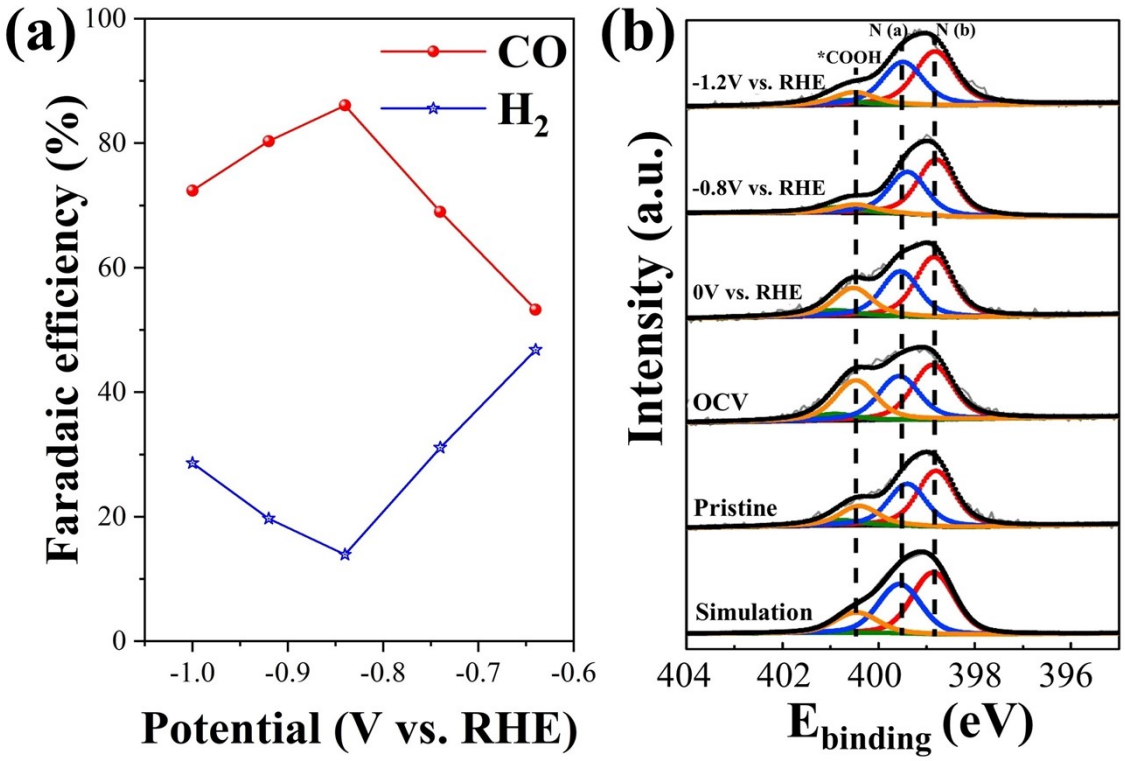

Fig. S16 (a)The Faraday efficiency of CO and H_2 for pure CoPc electrocatalytic CO_2RR. (b) The N 1s XPS spectra of CoPc at pristine, OCV, 0 V, -0.8V, -1.2V vs. RHE, respectively[5]

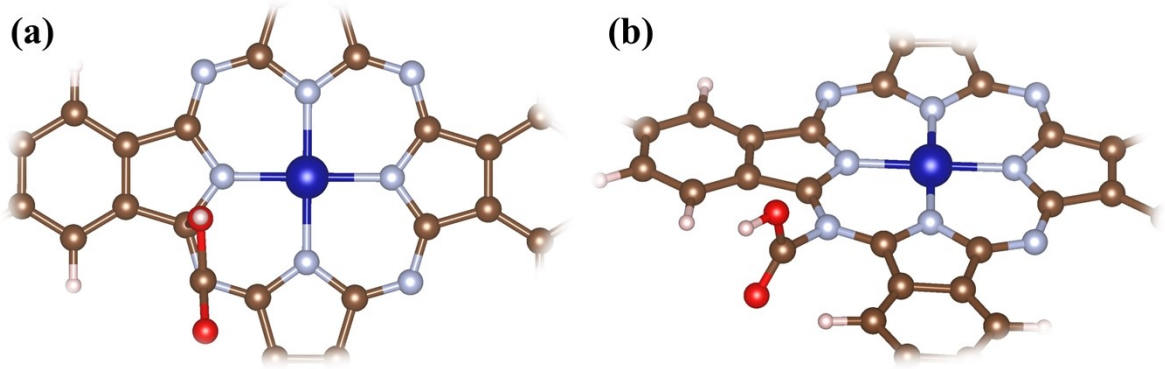

Fig. S17 (a-b) The configuration of the *COOH intermediate on the second nearest neighbor N site N (b) before and after geometry optimization.

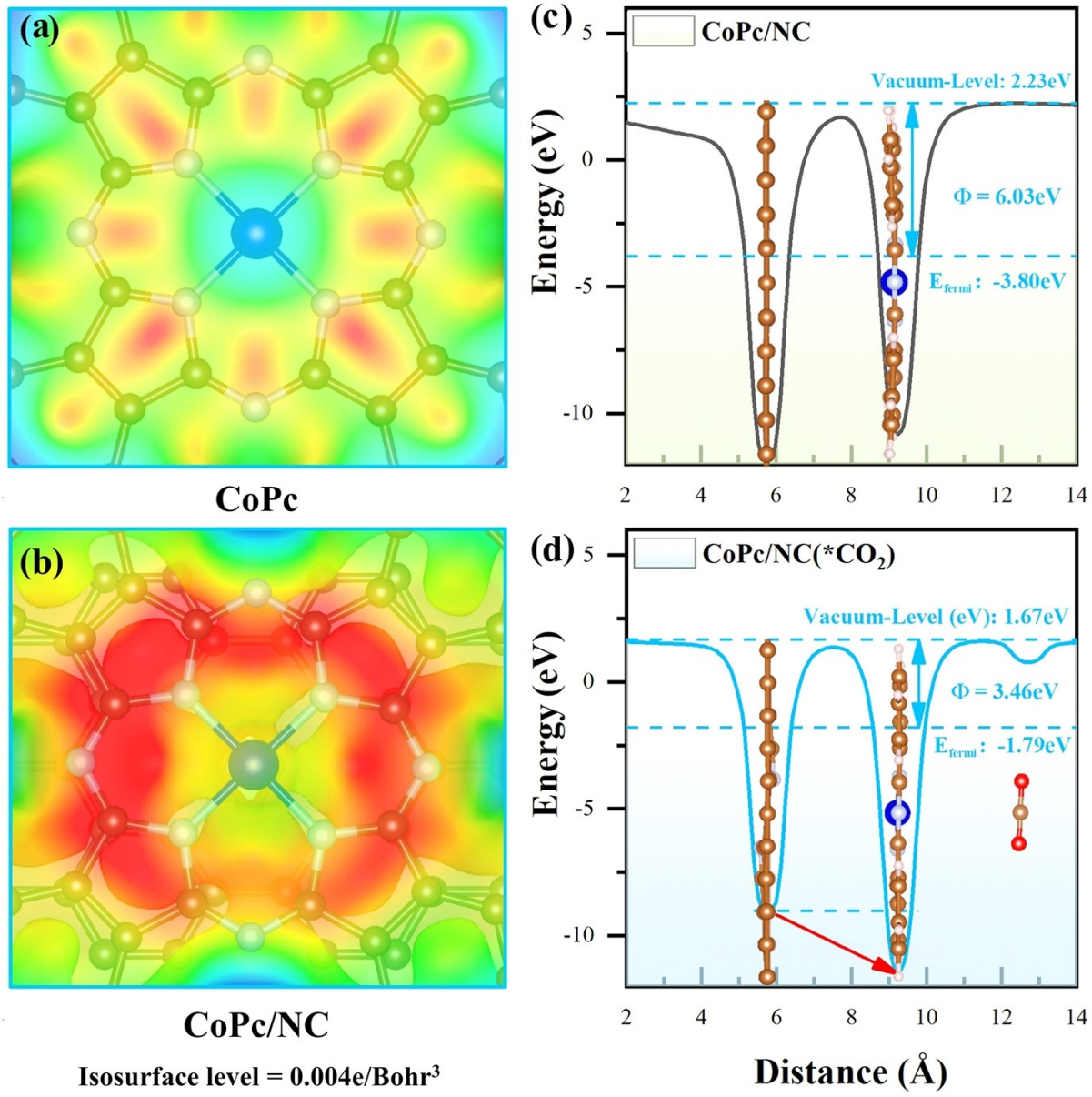

Fig. S18 (a-b) CoPc and CoPc/NC electrostatic potentials, respectively; (c-d) Work function of CoPc/NC catalyst before and after CO_2 adsorption.

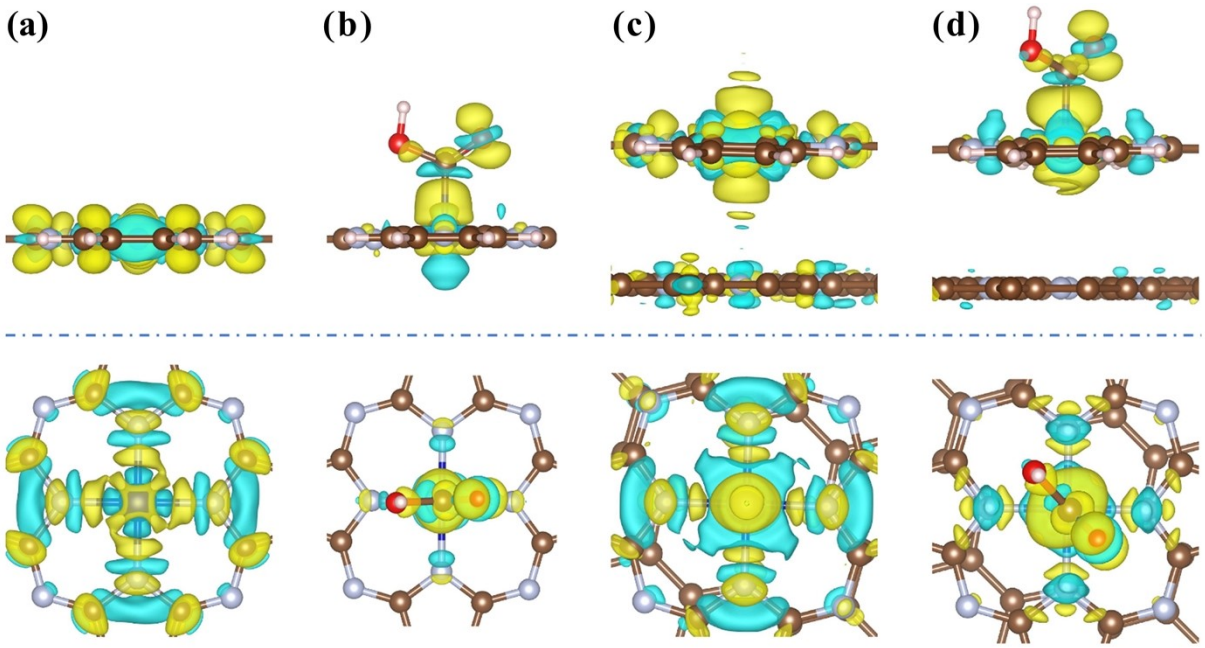

Fig. S19 (a-d) The side view and top view of the differential charge density of CoPc, CoPc-COOH, CoPc/NC and CoPc/NC-COOH, respectively.

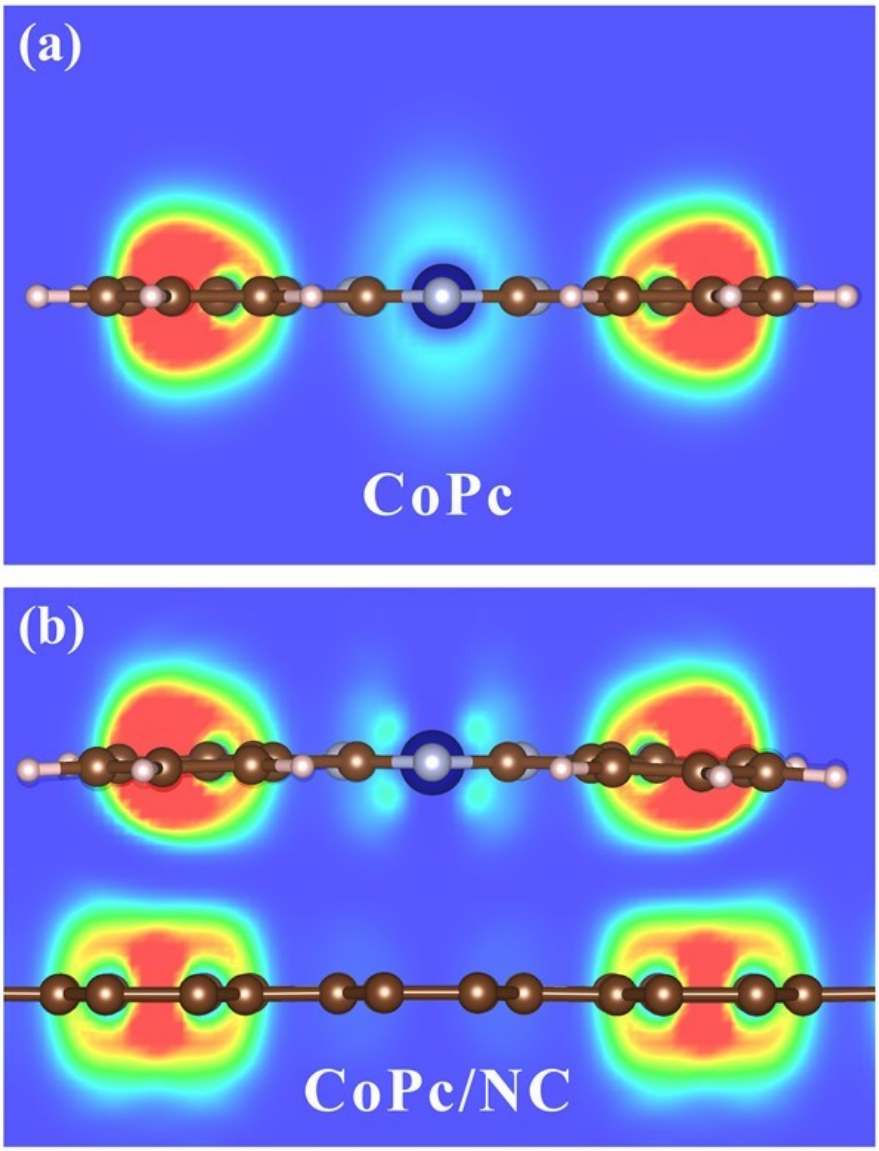

Fig. S20 ELF of CoPc (a) and CoPc/NC (b).

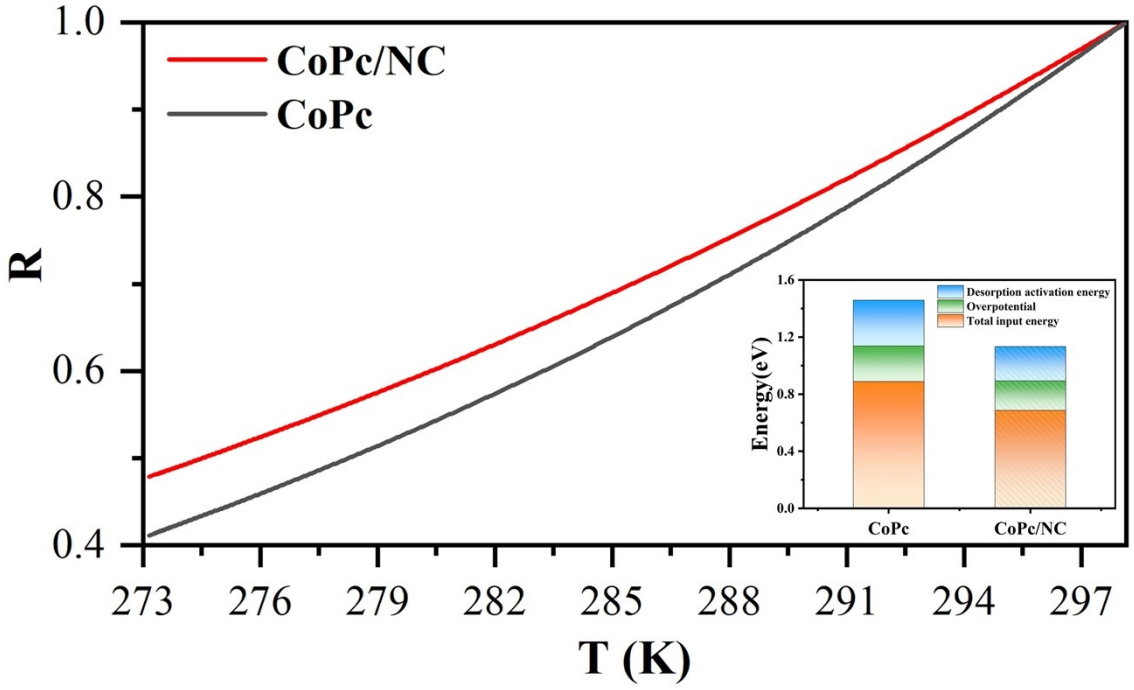

Fig. S21 The CO desorption reaction rate changes with temperature on CoPc and CoPc/NC, where the small illustrations show the comparison of the total input energy, desorption energy barrier and overpotential of CO_2RR on CoPc and CoPc/NC.

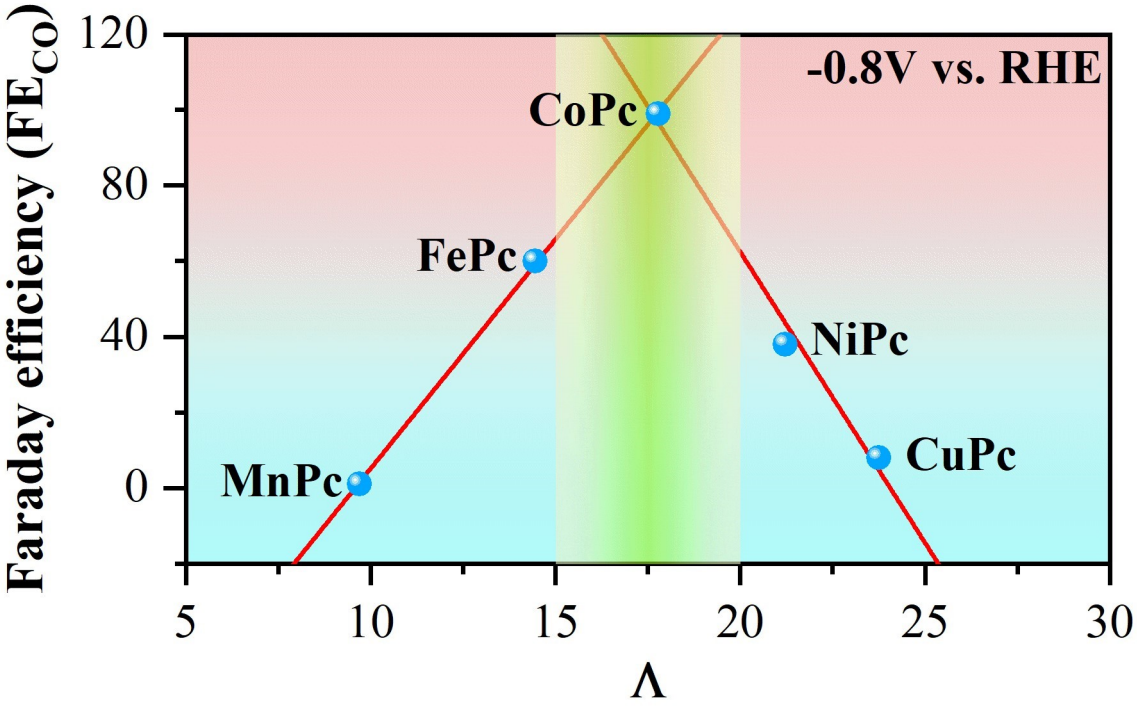

Fig. S22 The relationship between descriptor (Λ) and Faradaic efficiency (FE_{CO}) of M-Pc [6]

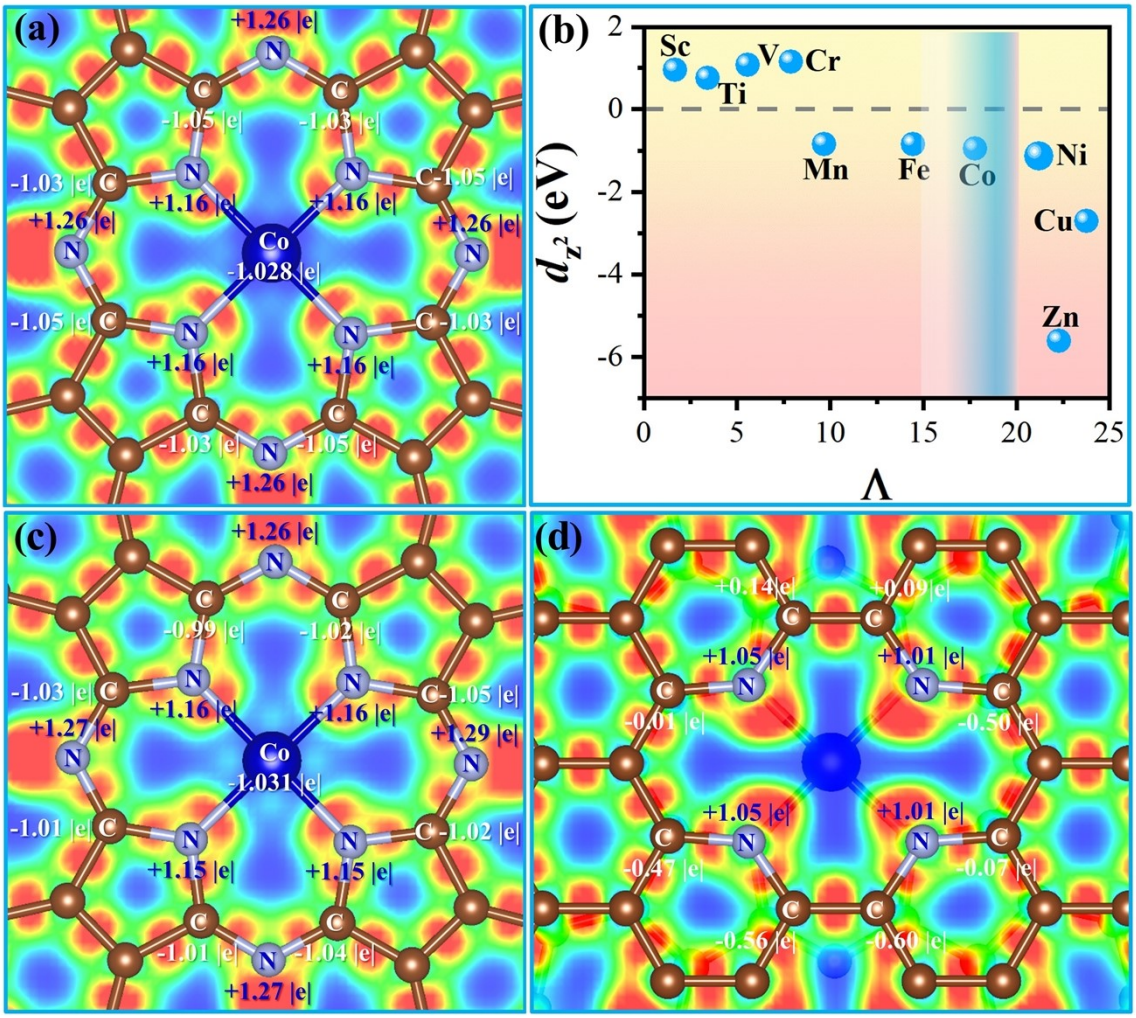

Fig. S23 (a) The Bader charge transfer on a CoPc is shown with the background picture of the electron location function of the CoPc model; (b) Bader charge on 3d-TMPc (inset) or 3d-TMPc/NC as a function of Λ; (c-d) The Bader charge transfer and electron localization function on the CoPc/NC bilayer are shown respectively.

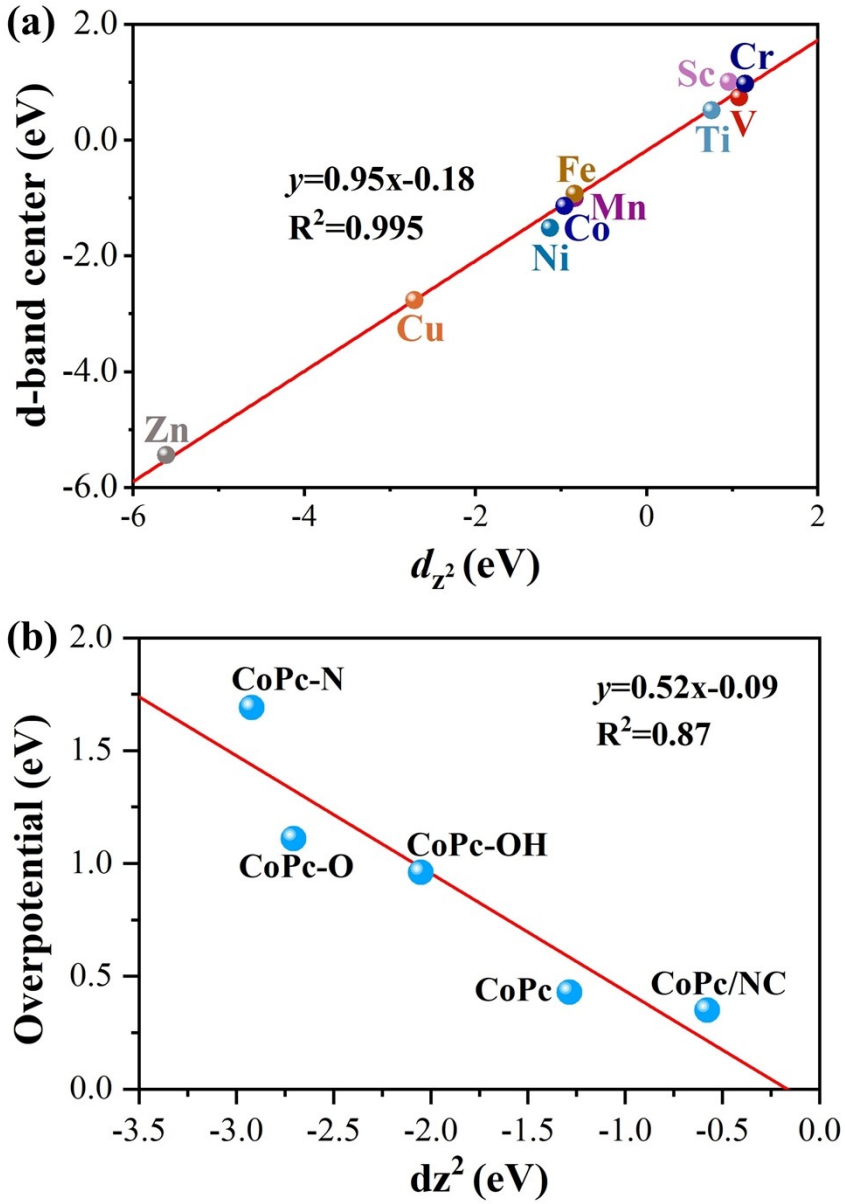

Fig. S24 (a) There is a linear relationship between d-band center and dz^2; (b) The relationship between the overpotential of CoPc and its various modified configurations (CoPc-N, CoPc-O, CoPc-OH and CoPc/NC) and dz^2.

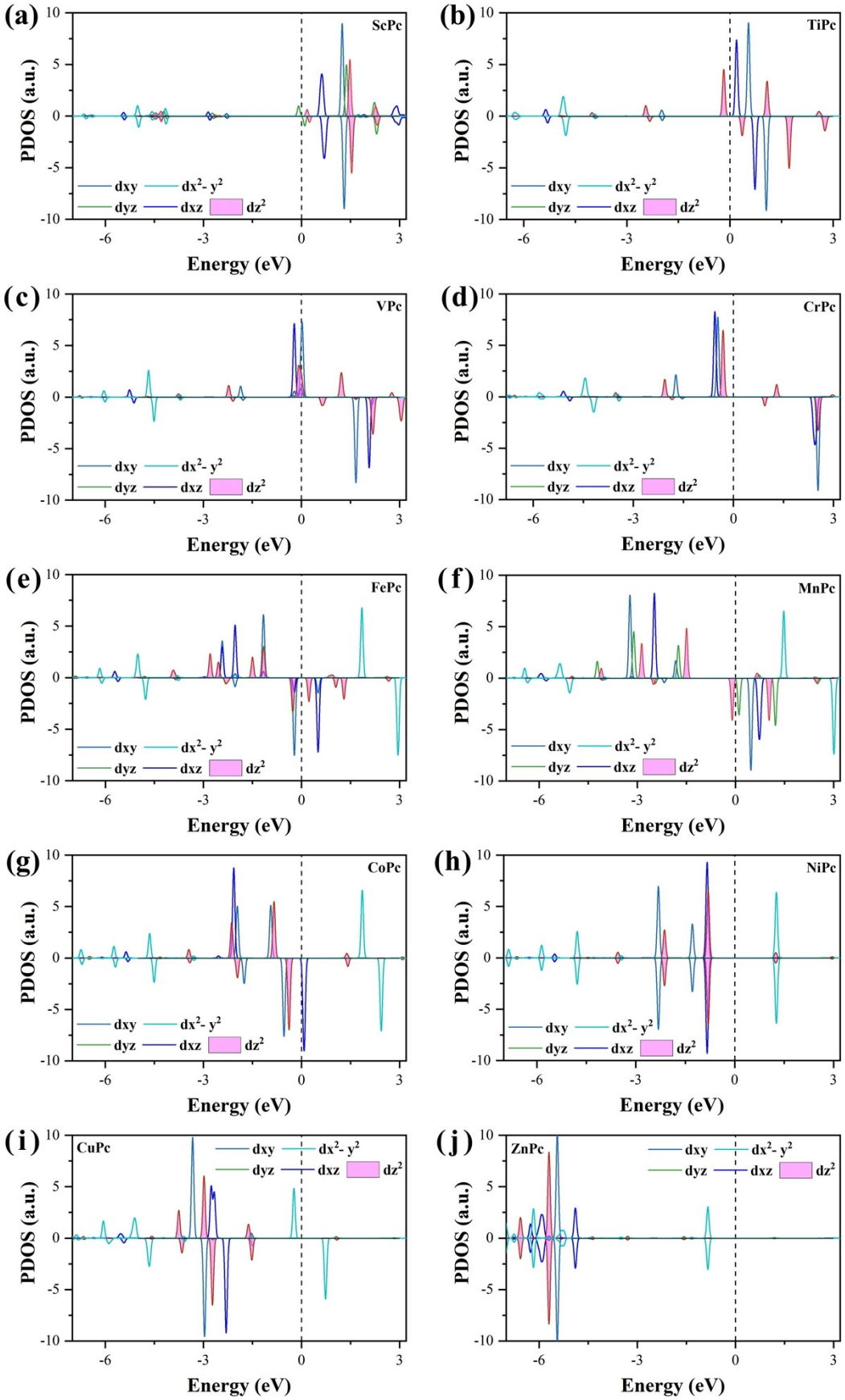

Fig. S25 The partial density of states of d orbitals of various 3d-TMPc catalysts.

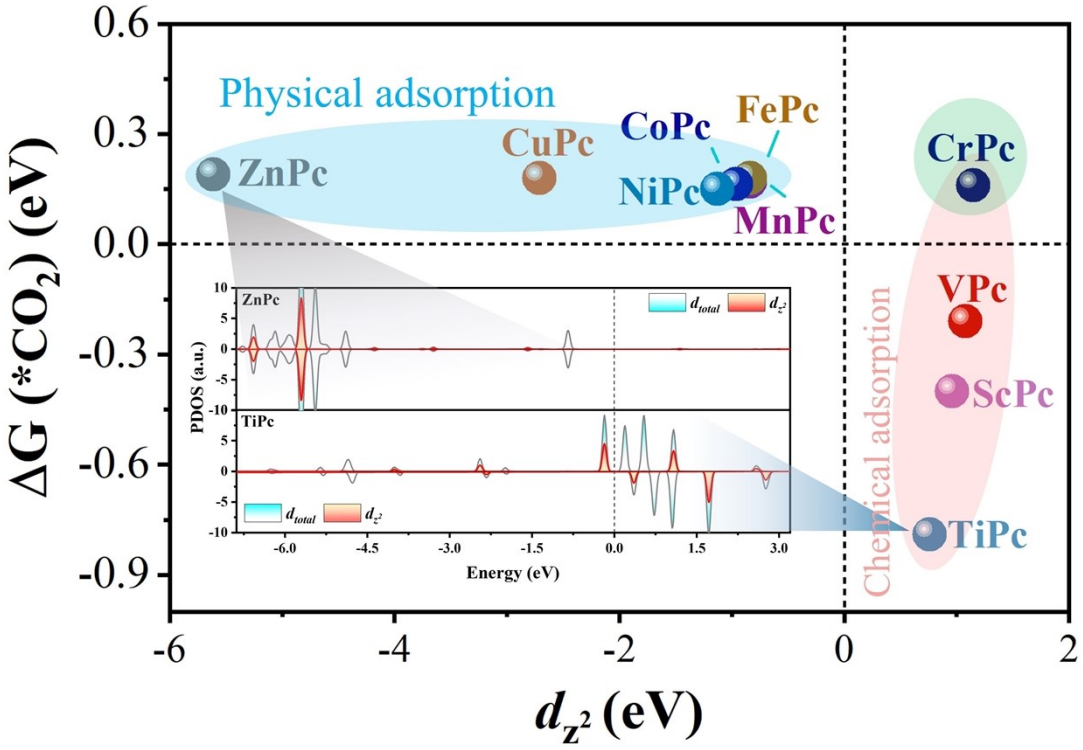

Fig. S26 The relationship between dz^2 and CO_2 adsorption free energy, in which the illustration compares the partial density of states of typical cases TiPc and ZnPc, and the higher dz^2 orbital energy is the key to adsorb CO_2 molecules.

Table S1. The binding energy (eV) of TMPc and cohesive energy (eV) of TM bulk.

	Sc	Ti	V	Cr	Mn	Fe	Co	Ni	Cu	Zn
E_{bind} (TMPc)	-10.82	-11.30	-10.57	-9.85	-9.40	-10.05	-10.45	-10.45	-7.79	-6.21
E_{bind} (TMPc/NC)	-17.31	-16.63	-14.77	-13.05	-12.66	-13.24	-13.64	-13.54	-10.92	-9.40
E_{coh} (TM bulk)	-4.27	-5.60	-5.37	-4.08	-3.75	-5.09	-5.53	-5.13	-3.47	-1.11

Table S2. Adsorption energy (eV) of *CO_2 and *H on TMPc.

	ScPc	TiPc	VPc	CrPc	MnPc	FePc	CoPc	NiPc	CuPc	ZnPc
E_{ads} (*CO_2)	-0.40	-0.79	-0.21	0.16	0.17	0.18	0.16	0.15	0.18	0.19
E_{ads} (*H)	-0.25	-0.46	-0.07	0.33	0.40	0.27	0.19	1.78	1.93	2.00

Table S3. The parameters of d-bend center (*d*) and the dz^2 orbital (dz^2).

	Sc	Ti	V	Cr	Mn	Fe	Co	Ni	Cu	Zn
d	1.00	0.51	0.74	0.97	-1.00	-0.93	-1.14	-1.52	-2.77	-5.44
dz^2	0.96	0.76	1.08	1.15	-0.84	-0.84	-0.96	-1.13	-2.71	-5.61

Table S4. The RLS, ΔG_{max} and η^{co} of CO_2RR in the TMPc structure where the active site is a transition metal atom.

TMPc	RDS	ΔG_{max}(eV)	η^{co} (V)
ScPc	*COOH → *CO	0.49	0.38
TiPc	*CO → * + CO	0.59	0.48
VPc	*CO → * + CO	0.68	0.57
CrPc	*+CO_2 → *CO_2	0.45	0.34
MnPc	*CO_2 → *COOH	0.61	0.50
FePc	*CO_2 → *COOH	0.46	0.35
CoPc	*+CO_2 → *CO_2	0.43	0.32
NiPc	*CO_2 → *COOH	1.90	1.79
CuPc	*CO_2 → *COOH	2.05	1.94
ZnPc	*CO_2 → *COOH	2.01	1.90

Table S5. The parameters of Ionic radius (r_{ion}), d electron number (E_n), electronegativity (N_d) and the the descriptor(Λ).

	Sc	Ti	V	Cr	Mn	Fe	Co	Ni	Cu	Zn
r_{ion} (Å)	0.81	0.90	0.88	0.84	0.80	0.76	0.74	0.72	0.72	0.74
E_n	1.36	1.54	1.63	1.66	1.55	1.83	1.88	1.91	1.90	1.65
N_d	1.00	2.00	3.00	4.00	5.00	6.00	7.00	8.00	9.00	10.00
Λ	**1.68**	**3.42**	**5.56**	**7.90**	**9.69**	**14.45**	**17.78**	**21.22**	**23.75**	**22.30**

References

1. G. L. Chai and Z. X. Guo, *Chem. Sci.*, 2016, **7**, 1268-1275.
2. L. Li, X. Chang, X. Lin, Z. J. Zhao and J. Gong, *Chem. Soc. Rev.*, 2020, **49**, 8156-8178.
3. H. Liu, J. Liu and B. Yang, *Chin. J. Catal.*, 2022, **43**, 2898-2905.
4. Z. Zhao and Z. Xia, *ACS Catal.*, 2016, **6**, 1553-1558.
5. Y. Xia, S. Kashtanov, P. Yu, L.-Y. Chang, K. Feng, J. Zhong, J. Guo and X. Sun, *Nano Energy*, 2020, **67**, 104163.
6. Z. Zhang, J. Xiao, X. J. Chen, S. Yu, L. Yu, R. Si, Y. Wang, S. Wang, X. Meng, Y. Wang, Z. Q. Tian and D. Deng, *Angew. Chem. Int. Ed.*, 2018, **57**, 16339-16342.